PAPER

CrossMark
click for updates

Metal binding spectrum and model structure of the *Bacillus anthracis* virulence determinant MntA†

Elena Vigonsky,‡[a] Inbar Fish,‡[b] Nurit Livnat-Levanon,[a] Elena Ovcharenko,[a] Nir Ben-Tal[b] and Oded Lewinson*[a]

The potentially lethal human pathogen *Bacillus anthracis* expresses a putative metal import system, MntBCA, which belongs to the large family of ABC transporters. MntBCA is essential for virulence of *Bacillus anthracis*: deletion of MntA, the system's substrate binding protein, yields a completely non-virulent strain. Here we determined the metal binding spectrum of MntA. In contrast to what can be inferred from growth complementation studies we find no evidence that MntA binds Fe^{2+} or Fe^{3+}. Rather, MntA binds a variety of other metal ions, including Mn^{2+}, Zn^{2+}, Cd^{2+}, Co^{2+}, and Ni^{2+} with affinities ranging from 10^{-6} to 10^{-8} M. Binding of Zn^{2+} and Co^{2+} have a pronounced thermo-stabilizing effect on MntA, with Mn^{2+} having a milder effect. The thermodynamic stability of MntA, competition experiments, and metal binding and release experiments all suggest that Mn^{2+} is the metal that is likely transported by MntBCA and is therefore the limiting factor for virulence of *Bacillus anthracis*. A homology-model of MntA shows a single, highly conserved metal binding site, with four residues that participate in metal coordination: two histidines, a glutamate, and an aspartate. The metals bind to this site in a mutually exclusive manner, yet surprisingly, mutational analysis shows that for proper coordination each metal requires a different subset of these four residues. ConSurf evolutionary analysis and structural comparison of MntA and its homologues suggest that substrate binding proteins (SBPs) of metal ions use a pair of highly conserved prolines to interact with their cognate ABC transporters. This proline pair is found exclusively in ABC import systems of metal ions.

Introduction

Trace metals such as $Cu^{1/2+}$, Zn^{2+}, Mn^{2+}, and $Fe^{2/3+}$ are essential cofactors to the structure and function of many enzymes and structural proteins, and it is estimated that metalloproteins comprise 30–40% of most proteomes.[1,2] However, since metal ions are toxic at high concentrations, all organisms must maintain a delicate balance between essential uptake and toxic overload.[3] This necessity places trace metals at the crossroads of host–pathogen interactions: to fight infections, hosts employ both metal sequestering/depravation and bombardment.[4–6] In turn, to maintain and control their intracellular metal quote, bacterial pathogens evolved elaborate uptake and extrusion systems. It is therefore not surprising that bacterial genes involved in metal homeostasis have been broadly demonstrated to be key virulence determinants.[7–10]

Bacterial pathogens primarily rely on their ATP Binding Cassette (ABC) transporters for the high-affinity acquisition of essential metals. This dependence is mirrored in the pivotal role of ABC transporters in bacterial virulence and pathogenesis. In many important human pathogens such as *Mycobacterium tuberculosis*,[11] *Staphylococcus aureus*,[12] *Streptococcus pneumoniae*,[13–15] *Salmonella typhi*,[16,17] *Streptococcus mutans*,[18] and *Yersinia pestis*[19] ABC importers of Zn^{2+}, Mn^{2+}, and $Fe^{2/3+}$ are essential to bacterial virulence and pathogenesis.

ABC transporters comprise a very large super-family of proteins.[20,21] They couple the energy of ATP hydrolysis to the energetically uphill translocation of molecules across biological membranes. These ubiquitous enzymes are present in all extant phyla with 79 genes in *E. coli*,[22] ~120 in higher plants,[23] and 48 in human.[24] The transported molecules are extremely diverse, ranging from small molecules (such as metal ions, sugars, amino acids) to large and bulky compounds (peptides, proteins, organo-metal complexes, and antibiotics).

ABC transporters consist minimally of four domains: two transmembrane domains (TMDs) and two cytoplasmic nucleotide-binding domains (NBDs).[25] Binding and hydrolysis of ATP at the NBDs power the translocation of substrates

[a] *Department of Biochemistry, The Bruce and Ruth Rappaport Faculty of Medicine Technion-Israel Institute of Technology, Haifa, Israel.*
E-mail: lewinson@tx.technion.ac.il; Fax: +972-4-8295205; Tel: +972-4-8295428

[b] *Department of Biochemistry and Molecular Biology, Tel-Aviv University, Tel-Aviv, Israel*

† Electronic supplementary information (ESI) available. See DOI: 10.1039/c5mt00100e

‡ These authors contributed equally.

through the permeation pathway formed by the TMDs. A given ABC transporter may function either as an exporter or an importer, with importers present only in prokaryotes. ABC transporters that function as importers depend on a high-affinity substrate binding protein (SBP) that delivers the substrate to the cognate transporter.[26–28]

The *mntBCA* operon of the potentially lethal human pathogen *Bacillus anthracis* encodes an ABC import system, putatively of manganese and/or iron. MntA (hereafter baMntA), the system's high-affinity substrate binding protein (SBP) is one of this pathogen's most important virulence determinants: its genetic deletion yields a completely non-virulent strain, less virulent than the Sterne strain used for vaccination.[29] Many other SBPs of ABC importers of iron, zinc, and manganese play significant roles in bacterial virulence,[8,11–13,15–19,30,31] but the effect of the baMntA deletion is the most dramatic, leading to a 50 000-fold increase in the LD_{50} of *Bacillus anthracis*. Remarkably, beyond its crucial role as a virulence determinant, very little is known of the structure and function of baMntA.

Here, we present the first structure–function analysis of baMntA. We determined its metal binding specificity and affinities, identified residues that participate in metal coordination, and describe a novel structural element that is likely required for the interaction of baMntA with its cognate ABC transporter.

Results

Overexpression and purification of baMntA

baMntA was cloned without its first 21 amino acids that code for the protein's membrane anchoring domain. To not interfere with subsequent metal binding measurements the protein was expressed without an affinity tag. *E. coli* were transformed with plasmid p-*mntA* and extracts were prepared before or after addition of IPTG. A prominent band of ~35 kDa (corresponding to the expected molecular weight of baMntA) was observed in SDS-PAGE of extracts prepared from induced cells (ESI,† Fig. S1A). For purification, cell extracts were subjected to ion exchange chromatography and gel filtration. This procedure yielded a preparation that was 80–90% pure (ESI,† Fig. S1B). The protein could be readily concentrated to 30 mg mL^{-1} (a process that improved its purity, ESI,† Fig. S1B) and was highly mono-disperse as judged by size exclusion chromatography (ESI,† Fig. S1C). Comparison of the elution volume of baMntA to the elution volumes (using the same column) of known molecular weight standards suggests that baMntA is a monomer (ESI,† Fig. S1D).

Metal binding selectivity of baMntA

Growth complementation studies implied that baMntA is the substrate binding protein (SBP) of a manganese/iron ABC metal uptake system.[29] We therefore began by characterizing the interaction of baMntA with Mn^{2+} and $Fe^{2/3+}$. Using Isothermal Titration Calorimetry (ITC) we readily detected a high affinity ($K_D = 3.6 \times 10^{-7}$ M) binding of Mn^{2+} by baMntA. The reaction is exothermic, and the data could be readily fitted using a simple 1 : 1 interaction model (Fig. 1A, see Methods for model fitting).

In contrast to the conclusions that may be drawn from the previously reported growth studies,[29] we could not detect binding of iron in either of its oxidation states ($Fe^{2/3+}$, Fig. 1B and C). Binding of iron was also not observed in the presence of reducing agent 2-mercaptoethanol. We next tested baMntA for its ability to bind a variety of other metals. We observed that in addition to Mn^{2+} baMntA also binds Cd^{2+}, Zn^{2+}, Co^{2+}, and Ni^{2+}. The metal binding affinities of baMntA ranged over nearly two orders of magnitude (Fig. 1D–F, ESI,† Table S1). The highest affinity was to Co^{2+} ($K_D = 5.2 \times 10^{-8}$ M) and the lowest to Ni^{2+} ($K_D = 4 \times 10^{-6}$ M). The binding affinities of baMntA to Cd^{2+} and Zn^{2+} were of intermediate values at 5.8×10^{-7} M and 2.9×10^{-7} M, respectively. In addition to $Fe^{2+/3+}$, we also did not detect binding of Mg^{2+} or Cu^{2+} (ESI,† Table S1). Rukhman *et al.* demonstrated that binding of Mn^{2+} by MntC of the cyanobacterium *Synechocystis* PCC is redox dependent, and is negatively affected by reducing agents.[32] This effect was attributed to the reduction of a disulfide bond that is unique to cyanobacterial SBPs of manganese. The two cysteines that form this bond are missing in baMntA and indeed binding of Mn^{2+} was unaffected by reducing agents (not shown).

Iron does not compete with manganese for binding to baMntA

The contradiction between the previously performed growth studies[29] and our inability to detect binding of either Fe^{2+} or Fe^{3+} prompted us to further investigate this issue. Lack of detection of iron binding may stem from limitations of the Isothermal Titration Calorimetry (ITC) approach. ITC measures heat released or absorbed during a reaction (enthalpy). It is therefore possible that if an association is driven mainly (or exclusively) by entropy it will not be detected by ITC. This is highly unlikely in the case of metal binding by baMntA, as metal binding by SBPs is strongly driven by enthalpy.[33–35] This is also specifically the case with baMntA, as binding of Mn^{2+}, Cd^{2+}, Zn^{2+}, Co^{2+}, and Ni^{2+} all have a strong enthalpic signature. To experimentally test whether iron binding occurs but is undetected in the ITC experiments we conducted binding competition experiments. Metal SBPs of ABC transporters such as baMntA have a single metal binding site (see also later) that binds a single metal ion at a time. Indeed, pre-incubation of baMntA with a molar excess of either Zn^{2+} or Co^{2+} completely abolished binding of Mn^{2+} (Fig. 2A and B), and identical results were obtained when Co^{2+} was injected into baMntA pre-incubated with Zn^{2+}. In contrast, pre-incubation of baMntA with a 10-fold molar excess of either Fe^{2+} or Fe^{3+} had no effect on Mn^{2+} binding, and the affinity of Mn^{2+} binding remained unchanged (Fig. 2C and D). Inhibition of Mn^{2+} binding by iron was also not observed in the presence of reducing agent 2-mercaptoethanol. Taken together, these results show that the metals that bind to baMntA do so in a mutually exclusive manner and that baMntA does not bind Fe^{2+} or Fe^{3+}.

A 3-D structural model of baMntA

To date, our efforts to determine the structure of baMntA by X-ray crystallography have failed. We therefore used comparative (homology) modeling to predict the structure of baMntA. A BLAST search of the protein data bank (PDB) identified MtsA
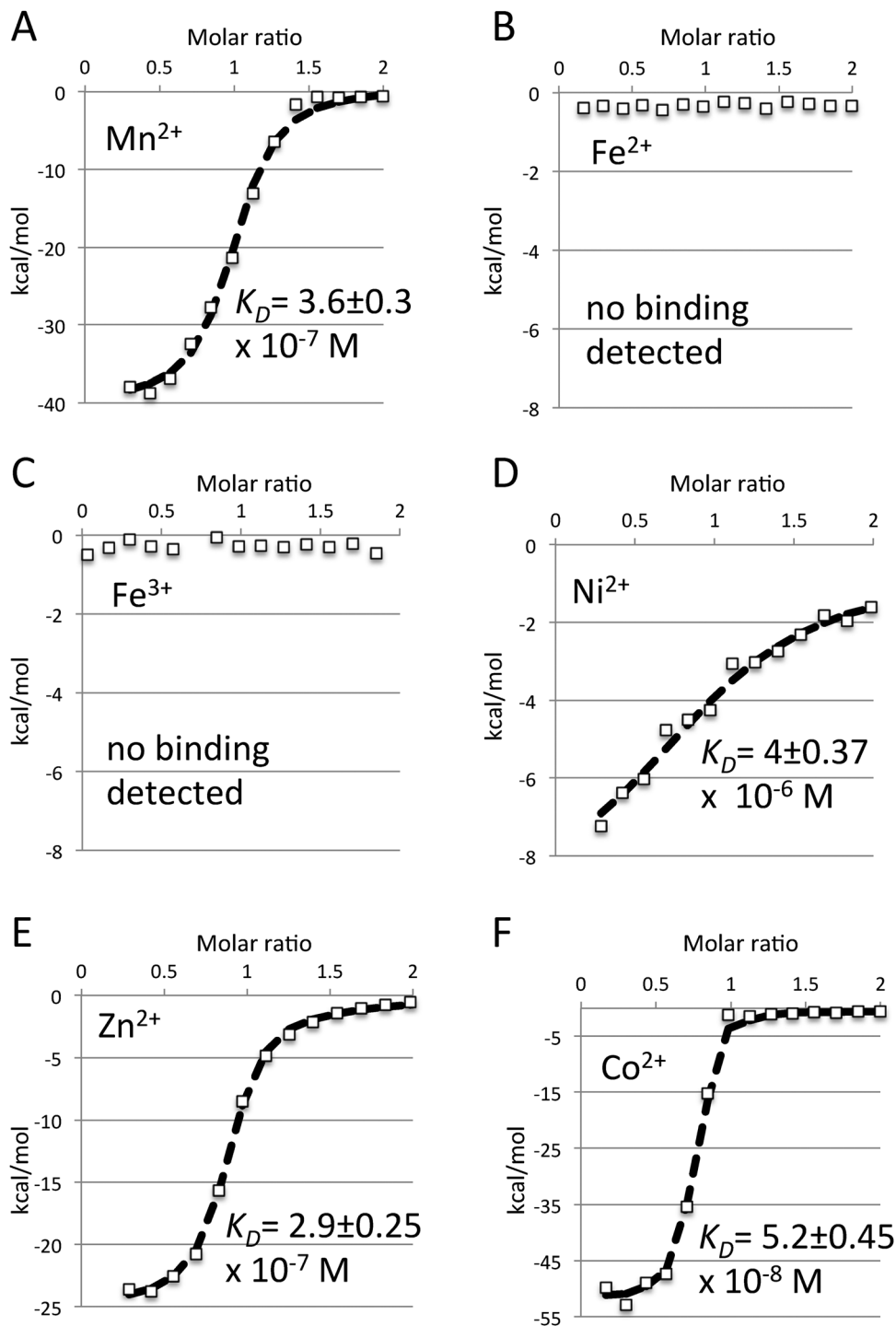
Fig. 1 The metal binding repertoire of baMntA. 2 μL aliquots from 0.2 mM of (A) $MnCl_2$ (B) $(NH_4)_2Fe(SO_4)_2$, (C) $FeCl_3$ (D) $Ni(SO_4)$ (E) $ZnCl_2$, (F) $CoSO_4$ were serially injected into a 200 μL solution of 15 μM baMntA. Changes in heat were recorded with a MicroCal iTC200 instrument. The open squares are the experimental data and the dashed line is the fit using a simple 1:1 binding model. Shown are representative ITC data of at least three repeats, the dissociation constant, and the standard errors of the fit to the data.

(PDB ID 3HH8) from *Streptococcus pyogenes*[36] as the most suitable template. The high sequence similarity between baMntA and spMtsA (53% identity, 90% similarity) and the similar functions[30] are indicative of the appropriateness of the template.

Three modeling tools were used to build a homology model of baMntA: MODELLER (version number 9.8),[37] I-TASSER,[38] and SWISS-MODEL.[39] Practically identical results were obtained using the three different algorithms (Fig. 3A), with RMSDs of 0.85–1.02 Å (backbone atoms) and 1.5–1.7 Å (whole atom comparison)
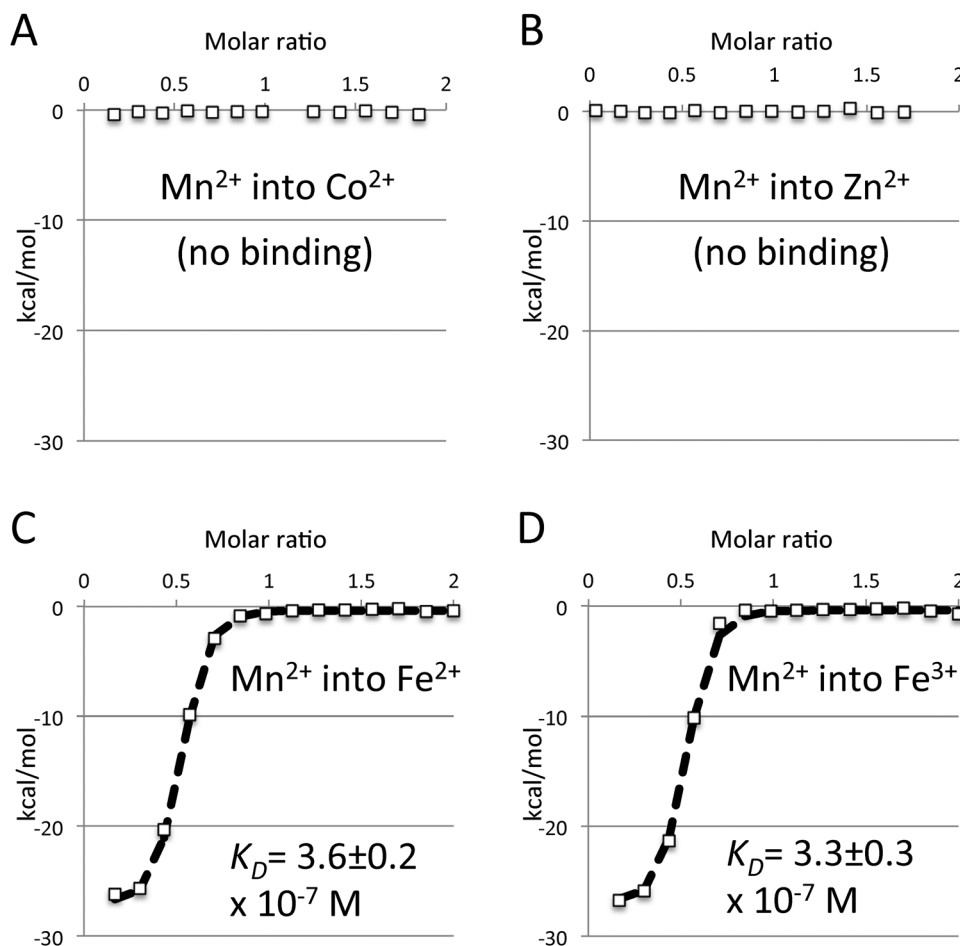
Fig. 2 Iron does not compete with Mn^{2+} for binding to baMntA. A 200 μL solution of baMntA (15 μM) was pre-incubated with 120 μM of (A) $CoSO_4$, (B) $ZnCl_2$, (C) $(NH_4)_2Fe(SO_4)_2$, or (D) $FeCl_3$. Subsequently, 2 μL aliquots of 0.2 mM $MnCl_2$ were serially injected and the changes in heat were recorded with a MicroCal iTC200 instrument. The open squares are the experimental data and the dashed line is the fit using a simple 1:1 binding model. Shown are representative ITC data of at least three repeats, the dissociation constant, and the standard errors of the fit to the data.
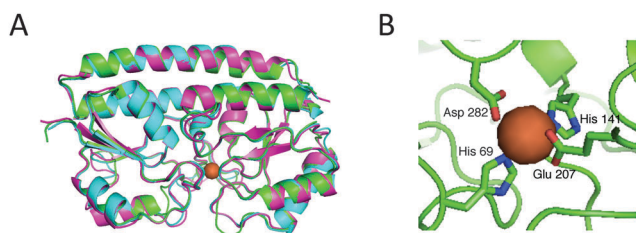

Fig. 3 Model structure of baMntA. (A) Structural alignment of the baMntA models created with MODELLER (green), SWISS-MODEL (cyan), or I-TASSER (magenta). MtsA (PDB ID 3HH8) was specified as a template for MODELLER. No template was specified for either SWISS-MODEL or I-TASSER. The protein is shown as a cartoon representation and the metal (here Zn^{2+}) as an orange sphere. (B) The proposed metal binding site of MntA (using MODELLER). His69, His141, Glu207, and Asp282 are intimately positioned to interact with the metal (Zn^{2+}, orange sphere).

between the three models. The model that was constructed with MODELLER was evaluated using three quality control programs. The stereo-chemical quality of the model was evaluated with PROCHECK,[40] the compatibility of the atomic model (3D) with its own amino acid sequence (1D) was evaluated

with Verify3D,[41] and the statistical (pseudo) energy potential of the model was computed with ProSA.[42] Highly similar Verify3D scores were obtained for the template and the model: 95.71% of the residues of the template had an average 3D-to-1D score > 0.2, whereas 96.79% of the residues in the model had an average score > 0.2. Ramachandran plot analysis shows that most of the residues are in allowed areas of the plot (ESI,† Fig. S2A), and the ProSA score of the model falls well within the allowed area and is highly similar to that of template (ESI,† Fig. S2B).

It is widely observed that the interior of proteins is much more evolutionarily conserved than their periphery.[43] We used the ConSurf webserver (http://consurf.tau.ac.il/) to validate that the model adheres to this anticipation (wrong models often do not[43]). As shown in ESI,† Fig. S2C, the ConSurf conservation analysis reveals a highly conserved core and an overall variable surface. The highest degree of conservation surrounds a central cavity, which is characteristic of binding sites. An extremely similar distribution of conserved and variable residues is also observed in the experimentally determined structures of the closely related SBPs MntC, PsaA, and MtsA (see later in Discussion and Fig. 5).

Not surprisingly, the overall predicted fold of baMntA is very similar to other metal ion SBPs.[32,36,44]

The model suggests the existence of a single metal binding site that is positioned in the interface between the N- and C-terminal domains of baMntA. Extensive loops surround the metal binding site and leave little unoccupied space. Four residues intimately interact with the metal: His69, His141, Glu207, and Asp282 (Fig. 3B). These four residues are invariably conserved in homologues of baMntA (ESI,† Fig. S3, and ref. 32, 36, 45 and 46). Three of these residues (His69, His141, Asp282) are conserved both in SBPs of Mn^{2+}/Fe^{2+} and in SBPs of Zn^{2+}. The fourth residue is glutamate in SBPs of Mn^{2+}/Fe^{2+} or histidine in SBPs of Zn^{2+} (ESI,† Fig. S3). In this respect, it is noteworthy that although this residue in baMntA is a glutamate (Glu207) it binds Mn^{2+}, Cd^{2+}, Zn^{2+} and Co^{2+} with high affinity but does not bind Fe^{2+}.

Role of conserved metal binding residues of baMntA

To test the involvement of the predicted residues in metal binding we generated single alanine substitutions. The mutant variants were overexpressed and purified as wild type baMntA and the Zn^{2+}, Co^{2+}, and Mn^{2+} binding affinities were measured in ITC experiments.

Quite surprisingly, the most dramatic effect was of the Glu207 substitution. This mutant (Glu207A) completely lost the ability to bind any of the tested metals (Table 1). Mutating His69 had the mildest effect: the mutant could still bind all three metals, albeit with reduced affinities ($\sim$10-fold reductions, Table 1). Substituting either His141 or D282 with alanine led to a selective loss of metal recognition: both mutants bound Zn^{2+} with near wild type affinities yet lost the ability to bind Co^{2+} or Mn^{2+}. Taken together, the simplest interpretation of these results is that although the metals bind to the same binding site, each of them binds in a different manner, and is differentially coordinated by residues of baMntA (see also below). Relative to its homologues, the metal binding site of baMntA is highly intolerant to substitutions. In both MtsA of *Streptococcus pyogenes*[36] and PsaA of *Streptococcus pneumoniae*[46] much milder effects were observed for similar substitutions.

Co^{2+}, Zn^{2+}, and Mn^{2+} bind differently to baMntA

The binding competition experiments shown in Fig. 2 show that metal binding to baMntA is mutually exclusive. In these experiments baMntA was first saturated with a molar excess of one metal and then injected with another. To further investigate the competition of metal binding we conducted experiments where we pre-incubated baMntA with one metal at a 1:1 molar ratio and then gradually injected a second metal to concentrations that surpass those of the first one. As shown, when baMntA was incubated with Mn^{2+} at a 1:1 molar ratio and then Zn^{2+} was gradually added, we still observed robust binding of Zn^{2+} (Fig. 4A). Analysis of the data using a simple competition model (see Methods for models) suggests that Zn^{2+} displaces pre-bound Mn^{2+} and that the Zn^{2+} $K_{D(apparent)}$ only mildly increases ($\sim$2-fold) in the presence of 15 µM Mn^{2+} (concentration of Mn^{2+} used in this experiment). Interestingly, analyzing the same data to determine the Mn^{2+} $K_{D(apparent)}$ suggests that Mn^{2+} is much more affected by Zn^{2+} than *vice versa*, its $K_{D(apparent)}$ increasing by $\sim$100-fold. This is surprising since individually both these metals bind to baMntA with very similar affinities. This asymmetry between Mn^{2+} and Zn^{2+} is further displayed by conducting the reverse experiment: titrating Mn^{2+} into baMntA that was pre-incubated with Zn^{2+} at a 1:1 molar ratio. As shown (Fig. 4B), under these conditions binding of Mn^{2+} was hardly observed, suggesting that once Zn^{2+} has bound it cannot be displaced by Mn^{2+}. Like Mn^{2+}, Co^{2+} hardly displaced pre-bound Zn^{2+}, despite the fact that it binds to baMntA with higher affinity than Zn^{2+} (Fig. 4C). This suggests that Zn^{2+} and Mn^{2+}, despite having similar binding affinities, bind differently to baMntA and that Mn^{2+} is released much more readily than Zn^{2+}. The unfavorable release of Zn^{2+} was also observed in experiments where baMntA was loaded with either Zn^{2+} or Mn^{2+} and then dialyzed against an EDTA-containing buffer. At intervals we withdrew samples and used inductively coupled plasma phase mass spectroscopy (ICP-MS) to measure the fraction of metal that remain bound. As shown (Fig. 4D), the two metals were released from baMntA at very different rates, with Mn^{2+} dissociating much faster than Zn^{2+}. Given that the two metals bind to baMntA with similar affinities (Fig. 1, ESI,† Table S1) this means that the association rate of Mn^{2+} to baMntA is much faster than that of Zn^{2+}. Kinetic experiments demonstrated that binding of Mn^{2+} by PsaA is a fast first-order reaction, while that of Zn^{2+} is a slow second-order reaction.[46] It seems that PsaA and baMntA that employ an identical set of metal-ligating residues share also this feature.

The differential interaction between baMntA and the metals was also studied by examining the effects of metal binding on thermostability. For this we used a fluorescence-based assay (SYPRO-orange) that has been extensively used to measure protein unfolding in general and specifically of substrate binding proteins of ABC transporters.[31,45,47–50] SYPRO-orange binds to

Table 1 Co^{2+}, Mn^{2+}, and Zn^{2+} binding affinities of wild type and mutant baMntA as determined by isothermal titration calorimetry (ITC). Also shown are the standard errors of the fit to the data

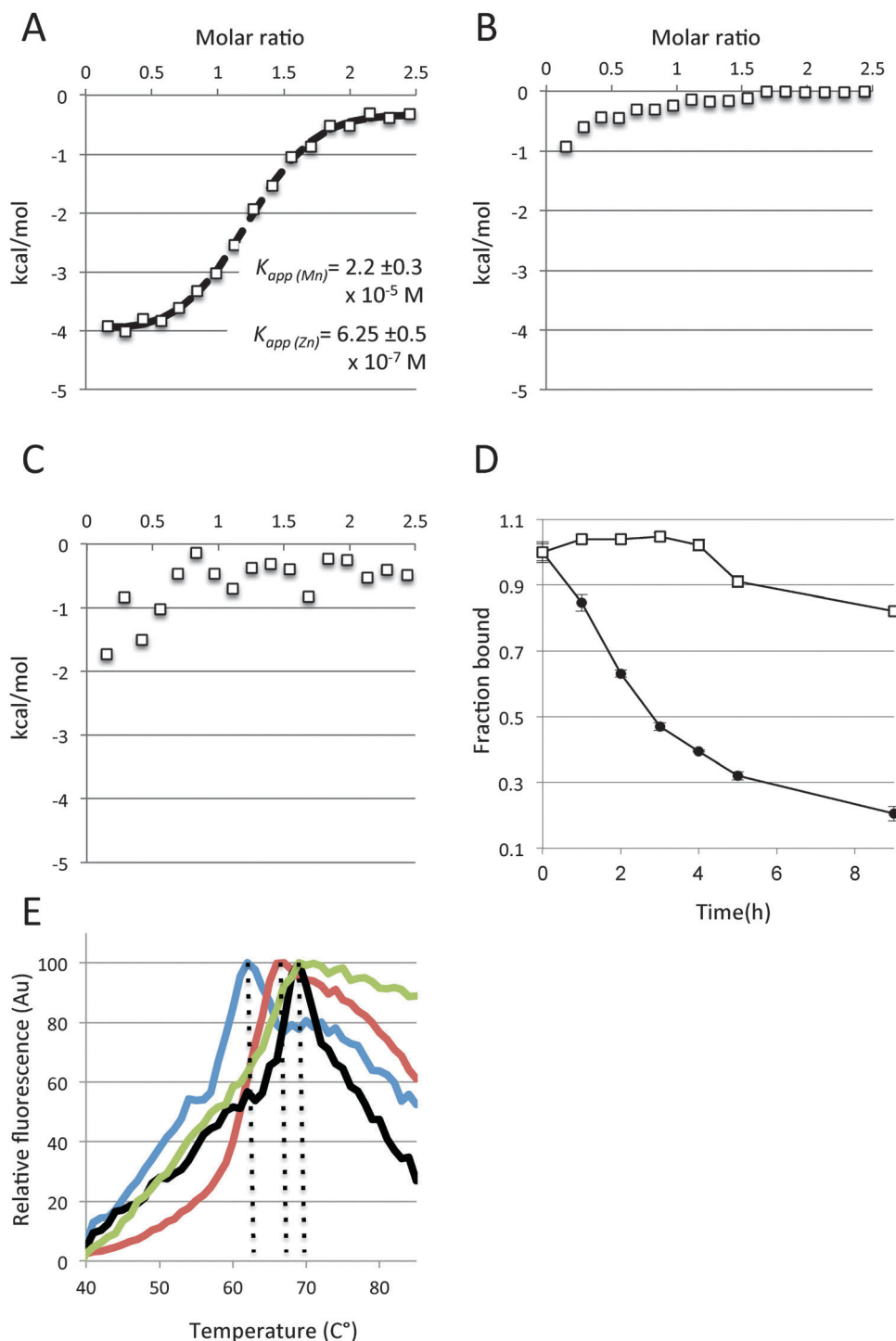|	K_D (M)		
	CoSO$_4$	MnCl$_2$	ZnCl$_2$
Wild type	$5.2 \pm 0.45 \times 10^{-8}$	$3.6 \pm 0.3 \times 10^{-7}$	$2.9 \pm 0.25 \times 10^{-7}$
His69Ala	$4.7 \pm 0.2 \times 10^{-7}$	$4.2 \pm 0.12 \times 10^{-6}$	$3.6 \pm 0.33 \times 10^{-6}$
His141Ala	No binding	No binding	$3.4 \pm 0.37 \times 10^{-7}$
Glu207Ala	No binding	No binding	No binding
Asp282Ala	Affinity too low to be determined	No binding	$3.1 \pm 0.28 \times 10^{-7}$

Fig. 4 Zn^{2+} and Mn^{2+} bind differently to baMntA. (A) A 200 µL solution of baMntA (15 µM) was pre-incubated with $MnCl_2$ at a 1:1 molar ratio. $ZnCl_2$ was then serially injected (each injection 2 µL from 0.2 mM stock). Changes in heat were recorded with a MicroCal iTC200 instrument. The open squares are the experimental data and the dashed line is the fit using a 1:1 competition model (see Methods) that accounts for the concentrations of both metals. (B) Same as in A, only the reciprocal experiment: baMntA was pre-incubated with $ZnCl_2$ at a 1:1 molar ratio and $MnCl_2$ was subsequently injected. (C) Same as in B, only baMntA was pre-incubated with $ZnCl_2$ at a 1:1 molar ratio and $CoSO_4$ was subsequently injected. (D) Mn^{2+} dissociates from baMntA much faster than Zn^{2+}. baMntA was incubated with either $ZnCl_2$ (white squares) or $MnCl_2$ (black circles) and then dialyzed (1000-fold) against a buffer that contained 20 mM EDTA. At the indicated intervals samples were withdrawn and the fraction of bound metal was determined by ICP-MS. Error bars (shown unless smaller than the icons) represent standard deviations of duplicates. (E) Thermostability of baMntA in the presence or absence of metals. baMntA (15 µM) was incubated with no metal (blue trace) or in the presence of a 1:1 molar ratio of $MnCl_2$ (red trace), $ZnCl_2$ (black trace), $CoSO_4$ (green trace). Shown is the change in SYPRO-orange fluorescence measured between 37–85 °C. The dashed lines indicate the temperature of peak fluorescence.
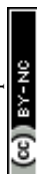
hydrophobic protein patches that are gradually exposed during heat denaturation and peak fluorescence is observed when the protein is fully denatured. Subsequently, as the protein begins to aggregate less hydrophobic surfaces are available for binding and the SYPRO-orange fluorescence declines.

For these thermo stability assays we first dialyzed baMntA against a 1000-fold excess of buffer containing 20 mM EDTA to remove any metals that might have been co-purified with the protein. In the absence of exogenously added metals, SYPRO-orange binding to EDTA treated baMntA displayed peak fluorescence at 62 °C. The temperature of peak fluorescence was shifted to 66 °C in the presence of Mn^{2+} (Fig. 4E), and a larger shift (to 69 °C) was observed in the presence of either Zn^{2+} or Co^{2+}. The irregularity of the slopes precluded the use of the first derivative to quantitate the mid-denaturation temperatures of apo and holo baMntA, as has been performed with PsaA from Streptococcus pneumoniae.[31,45] Nevertheless, despite the fact that absolute fluorescence values were used (rather than first derivatives) the effects of the different metals on the thermostability of baMntA are very similar to their effects on PsaA.[31,45] Taken together, the mutational analysis (Table 1) and the experiments shown in Fig. 4 suggest that although baMntA binds Mn^{2+}, Zn^{2+}, and Co^{2+} with similar affinities the geometry, chemistry, and stabilizing effects of the interactions are different.

A conserved protein:protein interaction surface in baMntA

Using the ConSurf algorithm we performed a structural conservation analysis of baMntA and compared it to that of three other SBPs of metal ions. A top view of baMntA reveals variability (not shown), as expected from a protein surface that is not engaged in functional interactions. In contrast, extensive patches of conserved structural elements are present at the bottom (cytoplasmic facing) of baMntA and its homologues (Fig. 5A). This conservation is partly due to the conserved metal binding site, but also to conserved elements that are positioned in the protein:protein interaction surface of the SBP with its transporter. Such extensive conservation on the face of the SBP that interacts with the transporter is also apparent in SBPs of Type-II ABC transporters such as BtuF, HmuT, and ShuT (Fig. 5B). However, it is largely absent in SBPs of Type-I ABC transporters such as MalE and HisJ (Fig. 5C). A pair of prolines stands out, (baMntA Pro44 and Pro204) and this proline pair is absolutely conserved in baMntA and its homologues, yet absent in SBPs of Type-I and Type-II transporters. The proline side chains point away from the SBPs and towards the transporter (Fig. 5D). Their location is reminiscent of that of the conserved glutamates of SBPs of Type-II ABC transporters (Fig. 5E), which are responsible for the high affinity interaction of the SBP with the transporter.[35,51,52] The central role of prolines in mediating protein:protein interactions is well-documented.[53] In this context, the orientation, location, and conservation of this pair of prolines suggests that they likely have a role in docking to the cognate ABC transporter(s).

Discussion

In recent years it is becoming increasingly clear that ABC transporters (importers) of d-block metals are crucial for bacterial virulence and pathogenesis.[3,11–19,29,30] This is perhaps not surprising as these trace elements are essential for bacterial growth yet their availability is very scarce in the host.[4] MntA of Bacillus anthracis presents an outstanding example of the great reliance of bacterial pathogens on their metal import systems. Deletion of mntA from the chromosome of Bacillus anthracis leads to complete arrest of Anthrax progression.[29] In fact, the resulting strain is less virulent than the one that is currently used for vaccination. It is very rare to find a single gene (that does not code for a virulence factor) with such a great contribution to virulence. We thus deemed it important to learn more of this metal import system.

baMntA is absolutely conserved (95–99% identity) in pathogenic strains of Bacillus anthracis and Bacillus cereus, yet a close homologue is absent from the non-pathogenic Bacillus subtilis. It is also absent from the chromosome of non-pathogenic E. coli strains, but present on a pathogenicity plasmid of the avian pathogenic E. coli (APEC). Closely related homologues (more than 50% identity) are also found in the pathogens Enterococcus faecalis, Enterococcus faecium, and Listeria monocytogenes. It thus seems that mntA homologues have been preserved in pathogenic bacteria.

Three metals are most commonly found at the crossroads of host–pathogen interactions: iron, zinc, and manganese. Iron and zinc are essential for countless bacterial physiological processes, including respiration, replication, translation, signaling, and cell division. Manganese is needed mainly for protection against oxidative stress, as a prosthetic group for superoxide dismutase (SOD) or directly conferring protection from oxidants. Oxidative stress is especially relevant for intracellular pathogens such as Bacillus anthracis as reactive oxygen species (ROS) are broadly used by the host as a defense mechanism. Additionally, the mammalian NRAMP transporters function to deprive pathogens of manganese by exporting this metal from the phagosomal lumen.[54] This may be especially relevant for Anthrax progression as spores of Bacillus anthracis are taken up by macrophages and the phagosome is the site of exit from spore state and initial germination.

One of the main goals of this work was to assess which metal is likely transported by MntBCA and thus presents the limiting factor for virulence of Bacillus anthracis. Previous studies showed that Bacillus anthracis ΔmntA fails to grow in defined media unless supplemented with either Mn^{2+} or Fe^{2+}. The complementation with Mn^{2+} was 5–10 times more efficient leading the authors to suggest that Mn^{2+} is the preferred substrate and that Fe^{2+} is transported with lower affinity.[29] We found no evidence for binding of Fe^{2+} or Fe^{3+} by baMntA. Moreover, high concentrations of Fe^{2+} or Fe^{3+} did not inhibit binding of Mn^{2+}. We therefore conclude at this point that $Fe^{2/3+}$ is most likely not transported by MntBCA. The genome of Bacillus anthracis encodes 7–10 ABC import systems for iron, heme, iron complexes, and iron-siderophores. This redundancy highlights the central role of iron in Bacillus anthracis metabolism and ensures iron availability in changing environments. The large repertoire of iron import systems, the dramatic effect of the mntA deletion, and our inability to detect iron binding all suggest that the ΔmntA strain did not turn a-virulent because it cannot acquire iron.
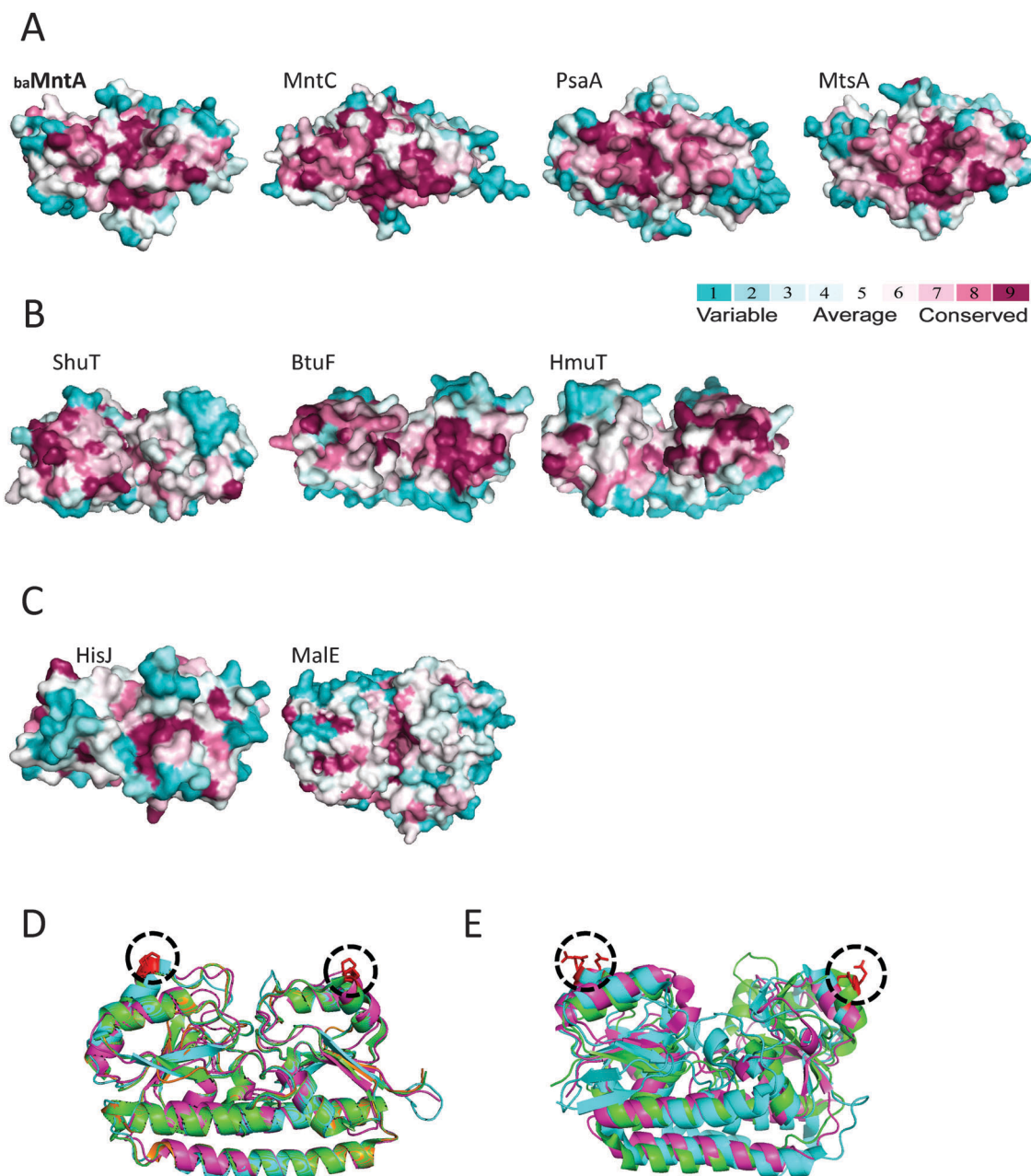
Fig. 5 A conserved interaction surface in baMntA. (A) Surface representation (bottom view) of a ConSurf analysis of the model structure of baMntA, and the crystal structures of MntC (PDB ID 1XVL), PsaA (PDB ID 1PSZ), and MtsA (PDB ID 3HH8). The least conserved residues are colored cyan, the most conserved are in purple. (B) Same as in A, but shown are the SBPs of Type-II ABC transporters ShuT (PDB ID 2R7A), BtuF (PDB ID 1N4A), and HmuT (PDB ID 3MD9). (C) Same as in A, but shown are the SBPs of Type-I ABC transporters HisJ (PDB ID 1HSL), and MalE (PDB ID 1ANF). (D) A cartoon representation of the structural alignment of baMntA (orange), MntC (magenta), PsaA (cyan), MtsA (green). The conserved prolines are colored red and circled. (E) Same as in D, shown is the structural alignment of HmuT (green), BtuF (magenta), and MolA (cyan). The conserved glutamates are colored red and circled.

baMntA binds both Mn^{2+} and Zn^{2+} with similarly high affinities and therefore both metals are possible transport substrates and potential contributors to virulence. Despite their similar binding affinities their binding by baMntA is not equivalent. Once Zn^{2+} has bound it cannot be replaced by Mn^{2+}, while the reciprocal displacement readily occurs. In addition, Mn^{2+} associates and dissociates much more readily than Zn^{2+}, and on the time-scale of transport reactions Zn^{2+} binding seems almost irreversible. Furthermore, Zn^{2+} has a greater thermo-stabilizing

effect on the protein than does Mn^{2+}. For a substrate to be efficiently transported (by any transport system) both its binding and release need to be reasonably fast. This does not seem to be the case for Zn^{2+} binding by baMntA. Very similar observations have been made with PsaA from *Streptococcus pneumoniae*[45,46] and SitA from *Staphylococcus pseudintermedius*.[55] Like these authors we suggest that Mn^{2+} and not Zn^{2+} is the transported metal. If this is correct, the direct conclusion is that the high affinity acquisition of Mn^{2+} presents a major barrier to the
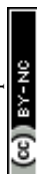
development of Anthrax. However, this proposal is currently speculative until verified by direct transport assays.

Unfortunately, we have so far failed in conducting biochemical studies of the complete transport system MntBCA (transporter + SBP). In fact, despite their clear importance, none of these ABC metal transporters have ever been characterized. From a mechanistic perspective we know very little about ABC transporters (importers) of metal ions. ABC importers display a diversity of transport mechanisms and are roughly divided to two mechanistic groups: Type I importers (of sugars, amino acids, peptides) and Type II importers (of vitamin B_{12}, heme, iron-siderophores).[25,51,56] However, this picture appears incomplete as recent reports of the ribose importer suggest the existence of a different, novel mechanism of action.[57] With respect to ABC importers of metal ions we have no knowledge if they operate by a mechanism that is similar to or different from those previously observed. Clues about their mechanism may be drawn from the structures of their substrate binding proteins (SBPs). SBPs of metal ions have the same fold as SBPs of vitamin B_{12}, heme, or iron-siderophores, a fold that is very different from that of SBPs of sugars, amino acids, or peptides.[3,34,58] The structures of the cognate ABC transporters are shaped according to the SBPs,[25,59–61] and therefore one may infer that the structure of ABC transporters of metal ions is similar to that of Type II importers. This hypothesis is supported to an extent by the model structure of MntBC (Fig. 6A). We used 5 different programs to predict the structure of MntBC: MODELLER, SWISS-MODEL, HHPred, FFAS03, and I-TASSER. Practically identical structures were predicted by all 5 programs, and the whole atom RMSDs for the membrane domain was between 0.28 and 1.65 Å. In further support of the MntBC model, a ConSurf analysis shows the presence of a highly conserved membrane permeation pathway surrounded by variable residues that face the membrane (Fig. 6B).

The model predicts the presence of 8 transmembrane helices per MntC monomer (16 helices in the assembled transporter), and the same result was obtained by using the TMHMM prediction tool.[62] The presence of 8 transmembrane helices per monomer is intermediate between 10 transmembrane helices of Type-II transporters such as BtuCD[63] and 5–6 transmembrane helices in Type-I transporters such as MetNI.[64] With respect to the number of amino acids that compose the TMDs, ABC transporters of metal ions are right between the 'big' Type-II transporters and the 'small' Type-I transporters: e.g., BtuC (326 amino acids), MntC (288 amino acids), and MetI (217 amino acids).

A structural element that is plainly missing from ABC transporters of metal ions is the "knobs and pockets" feature of Type II importers. Invariant glutamates (knobs) on the SBPs of Type II systems snugly fit into an arginine pocket of the transporter.[52,60] This interaction is responsible for the high affinity complexes formed between Type II importers and their cognate SBPs.[35,51] The high affinity and stability of the transporter–SBP complex is the mechanistic hallmark of Type II importers, and the stability of this complex dictates the transport mechanism. Type I importers completely lack theses "knobs and pockets" and indeed do not form high affinity
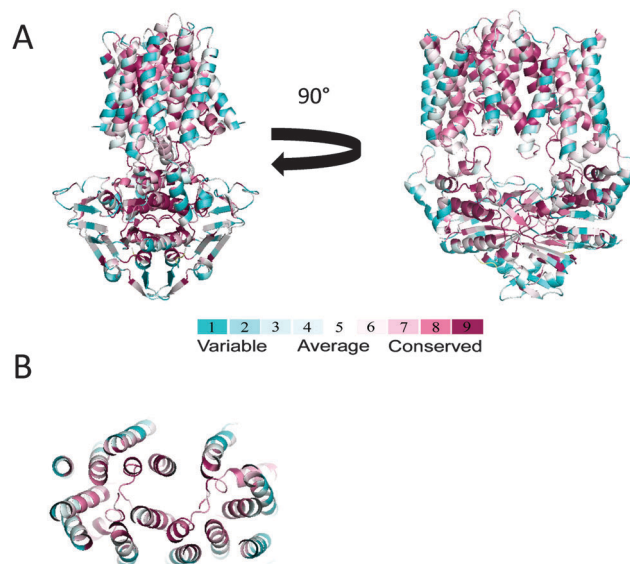

Fig. 6 Model structure of baMntBC. (A) The transporter complex, consisting of the nucleotide-binding domain (MntB) and the transmembrane domain (MntC) was modeled with MODELLER using the structure of MolBC (PDB ID 2NQ2) as a template. Left and right panels are side views rotated by 90°. The protein backbone is shown as a cartoon representation colored according to the ConSurf scale (most variable residues in cyan, most conserved in purple). (B) A top view of the trans-membrane domain formed by the MntC dimer. Shown is a slab view at approximately the middle of the membrane plane, with MntB (the nucleotide binding domain) removed for clarity.

transporter–SBP complexes, and thus operate by a very distinct mechanism.[35,65–70] In this context, ABC transporters of metal ions may present a middle ground: they lack the glutamates–arginines interaction but instead have a pair of prolines that is perfectly positioned to mediate protein:protein interactions. Clearly, mechanistic studies of this important yet uncharacterized group of ABC transporters are much needed.

The results we report here, and the identification of mutants of baMntA with a selective (or full) loss of metal binding provide an important stepping stone for future studies of *Bacillus anthracis* virulence and Anthrax progression in animal models.

Materials and methods

MntA cloning, expression and purification

The mntA gene from *Bacillus anthracis* was cloned into pET-19b (Novagen) vector for expression without its N-terminal lipid-anchoring domain (first 21 amino acids). baMntA was expressed in *E.coli* BL21-Gold(DE3) cells (Stratagene) using either M9 minimal media or Terrific Broth, as indicated in the text. Protein expression was induced at mid log phase by addition of 1 mM Isopropyl β-D-1-thiogalactopyranoside (IPTG) at 37 °C for 2 h. Cells were harvested by centrifugation (13 600 × g, 20 min, 4 °C) and the pellet was stored at −80 °C until use.

For baMntA purification, cells were homogenized in 20 mM Tris-HCl pH 8, 10 mM NaCl, complete EDTA-free protease inhibitor (Roche), 30 μg mL^{-1} DNase (Worthington), 1 mM
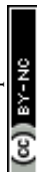
$CaCl_2$ and 1 mM $MgCl_2$ and ruptured by three passages in an EmulsiFlex-C3 homogenizer (Avestin). The lysate was ultra-centrifuged at 350 000 × g, 30 min, 4 °C and the supernatant was loaded onto anion-exchange column (Resource Q 1 mL, GE Healthcare). The unbound fraction, containing baMntA, was collected and further purified by size-exclusion chromatography (HiLoad 16/600, GE Healthcare). Protein purification was monitored by coomassie staining of SDS-PAGE and size-exclusion chromatography (SEC).

Structural modeling

We searched the baMntA sequence against the PDB database using blastp (protein–protein BLAST). The structure of MtsA (PDB ID 3HH8) was the most relevant template with high sequence identity (53%). We constructed several multiple sequence alignments (MSAs) using different techniques and parameters in order to get the best alignment. This included collecting homologous sequences *via* an HMMER search[71] against the UniProt and SwissProt databases. In addition we conducted PSI-BLAST[72] searches against the UniProt, SwissProt, and clean_UniProt with one, two or three iterations. The collected sequences in all cases were aligned using the MUSCLE algorithm.[73] We then extracted the aligned sequences of baMntA and MtsA from the different MSAs to obtain additional pairwise alignments. Reassuringly, all the pairwise alignments were indeed similar, as anticipated owing to the high sequence identity. We then used this pairwise alignment to build a model using MODELLER. Modeling of baMntA with SWISS-MODEL[39] and I-TASSER[38] was performed in automated mode, without specifying a template, using the default parameters of both programs.

We used the same procedures as the modeling of baMntA to model MntB and MntC. For MntB we used PDB ID 2NQ2, chain C (30% seq id, 89% query cover, *e*-value 1*e*-32). For MntC we used PDB ID 2NQ2, chain A (14% seq id, 97% query cover, *e*-value 2*e*-15).

Construction and purification of MntA mutants

Point mutations (H69A, H141A, E207A, D282A) were introduced into wild type baMntA by using QuikChange Lightning site-directed mutagenesis kit (Agilent Technologies). Mutations were confirmed by sequence analysis. Mutant proteins were overexpressed and purified as the wild type baMntA.

Isothermal titration calorimetry

Calorimetric measurements were performed with MicroCal iTC200 System (GE Healthcare). Metals stocks were dissolved in double-distilled water (except for Fe^{2+} in 1% H_2SO_4 and Fe^{3+} in 2% HCl) and diluted into the buffer of the experiment (25 mM Tris-HCl pH 8, 150 mM NaCl). All measurements were carried out at 25 °C. 2 μL aliquots of metal (0.2–0.6 mM, as indicated) were added by a rotating syringe to the reaction well containing 200 μL of 15–60 μM (as indicated) baMntA. Data fitting was performed with the AFFINImeter server (http://www.affinimeter.com). Unless stated otherwise the experimental data was fit using a simple 1 : 1 binding model, where the metal free form of the protein (FS) is in equilibrium with the bound species (MA): FS ⇔ MA. For the competition

experiments shown in Fig. 4 the data was fit using the Competitive model of AFFINImeter, where the metal free form of the protein (FS) is in equilibrium with the bound species (MA) and a second bound species (MB): MA FS ⇔ MB.

EDTA treatment of baMntA

For the metal release experiments 1.4 mL of baMntA (75 μM) were incubated with 50 μM of the indicated metal for 10 minutes at room temperature. The mixture was then placed in a dialysis tube (D-tube Dialyzer, MWCO 6–8 kDa, Novagen) and dialyzed against 1.4 L of 25 mM Tris-HCl pH 8, 150 mM NaCl and 20 mM EDTA at 4 °C. At the indicated intervals 0.2 mL samples were withdrawn and diluted 15-fold with double distilled water. The metal content of baMntA was determined by ICP-MS.

Thermal shift assay

15 μM baMntA were mixed with metal ion (Mn^{+2}, Zn^{+2} or Co^{+2}) in a 1 : 1 molar ratio and SYPRO Orange (Molecular probes) was added at 0.5× of the manufacturer's guidelines. 20 μL were subjected to thermal unfolding from 25 °C to 85 °C at a heating rate of 1 °C per min, using a Corbett real-time cycler (Rotor Gene 6000). Fluorescence was recorded by excitation at 470 and emission at 610. Data were also collected for buffer only, protein without metal ions and for each of the metal ions without protein. After subtraction of the buffer fluorescence from that of the protein containing samples, the relative fluorescence was plotted against the temperature.

Inductively coupled plasma mass spectrometry (ICP-MS)

Metal ions content was determined by ICP-MS, at the Earth Science institute (Hebrew university of Jerusalem). Samples were diluted to a final concentration of 5 μM in 1% HNO_3 and analyzed by ICP-MS using Agilent 7500cx ICP-MS. Each sample was measured three times and averaged.

Conflicts of interest

The authors declare no conflict of interest.

Acknowledgements

References

1 C. Andreini, *et al.*, MetalPDB: a database of metal sites in biological macromolecular structures, *Nucleic Acids Res.*, 2013, **41**(D1), D312–D319.
2 C. Andreini, *et al.*, Metal ions in biological catalysis: from enzyme databases to general principles, *JBIC, J. Biol. Inorg. Chem.*, 2008, **13**(8), 1205–1218.
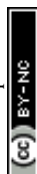
3 J. S. Klein and O. Lewinson, Bacterial ATP-driven transporters of transition metals: physiological roles, mechanisms of action, and roles in bacterial virulence, *Metallomics*, 2011, **3**(11), 1098–1108.

4 K. W. Becker and E. P. Skaar, Metal limitation and toxicity at the interface between host and pathogen, *FEMS Microbiol. Rev.*, 2014, **38**(6), 1235–1249.

5 T. E. Kehl-Fie and E. P. Skaar, Nutritional immunity beyond iron: a role for manganese and zinc, *Curr. Opin. Chem. Biol.*, 2010, **14**(2), 218–224.

6 V. E. Diaz-Ochoa, *et al.*, Transition metal ions at the crossroads of mucosal immunity and microbial pathogenesis, *Front. Cell. Infect. Microbiol.*, 2014, **4**, 2.

7 K. M. Papp-Wallace and M. E. Maguire, Manganese Transport and the Role of Manganese in Virulence, *Annu. Rev. Microbiol.*, 2006, **60**(1), 187–209.

8 M. I. Hood, *et al.*, Identification of an Acinetobacter baumannii Zinc Acquisition System that Facilitates Resistance to Calprotectin-mediated Zinc Sequestration, *PLoS Pathog.*, 2012, **8**(12), e1003068.

9 G. Porcheron, *et al.*, Iron, copper, zinc, and manganese transport and regulation in pathogenic Enterobacteria: correlations between strains, site of infection and the relative importance of the different metal transport systems for virulence, *Front. Cell. Infect. Microbiol.*, 2013, **3**, 90.

10 C. Guilhen, M.-K. Taha and F. J. Veyrier, Role of transition metal exporters in virulence: the example of Neisseria meningitidis, *Front. Cell. Infect. Microbiol.*, 2013, **3**, 102.

11 G. M. Rodriguez and I. Smith, Identification of an ABC Transporter Required for Iron Acquisition and Virulence in Mycobacterium tuberculosis, *J. Bacteriol.*, 2006, **188**(2), 424–430.

12 B. A. Diep, *et al.*, Identifying potential therapeutic targets of methicillin-resistant Staphylococcus aureus through in vivo proteomic analysis, *J. Infect. Dis.*, 2014, **209**(10), 1533–1541.

13 J. S. Brown, *et al.*, Characterization of Pit, a Streptococcus pneumoniae Iron Uptake ABC Transporter, *Infect. Immun.*, 2002, **70**(8), 4389–4398.

14 A. Marra, *et al.*, In vivo characterization of the Psa genes from Streptococcus pneumoniae in multiple models of infection, *Microbiology*, 2002, **148**(5), 1483–1491.

15 A. Dintilhac and J. P. Claverys, The ADC locus, which affects competence for genetic transformation in Streptococcus pneumoniae, encodes an ABC transporter with a putative lipoprotein homologous to a family of streptococcal adhesins, *Res. Microbiol.*, 1997, **148**(2), 119–131.

16 S. Ammendola, *et al.*, High-Affinity Zn^{2+} Uptake System ZnuABC Is Required for Bacterial Zinc Homeostasis in Intracellular Environments and Contributes to the Virulence of Salmonella enterica, *Infect. Immun.*, 2007, **75**(12), 5867–5876.

17 T. Pattery, J. P. Hernalsteens and H. De Greve, Identification and molecular characterization of a novel Salmonella enteritidis pathogenicity islet encoding an ABC transporter, *Mol. Microbiol.*, 1999, **33**(4), 791–805.

18 S. Paik, *et al.*, The sloABCR Operon of Streptococcus Mutans Encodes an Mn and Fe Transport System Required for Endocarditis Virulence and its Mn-dependent Repressor, *J. Bacteriol.*, 2003, **185**(20), 5967–5975.

19 S. W. Bearden and R. D. Perry, The Yfe system of Yersinia pestis transports iron and manganese and is required for full virulence of plague, *Mol. Microbiol.*, 1999, **32**(2), 403–414.

20 C. F. Higgins, ABC transporters: from microorganisms to man, *Annu. Rev. Cell Biol.*, 1992, **8**, 67–113.

21 I. B. Holland, *et al.*, in *ABC Proteins: From Bacteria to Man*, ed. I. B. Holland, Academic Press, London, 2003, p. 647.

22 K. J. Linton and C. F. Higgins, The Escherichia coli ATP-Binding Cassette (ABC) proteins, *Mol. Microbiol.*, 1998, **28**(1), 5–13.

23 R. o. Sánchez-Fernández, *et al.*, The Arabidopsis thaliana ABC Protein Superfamily, A Complete Inventory, *J. Biol. Chem.*, 2001, **276**(32), 30231–30244.

24 M. Dean, Y. Hamon and G. Chimini, The human ATP-binding cassette (ABC) transporter superfamily, *J. Lipid Res.*, 2001, **42**(7), 1007–1017.

25 D. C. Rees, E. Johnson and O. Lewinson, ABC transporters: the power to change, *Nat. Rev. Mol. Cell Biol.*, 2009, **10**(3), 218–227.

26 G. F. Ames, *et al.*, Traffic ATPases: a superfamily of transport proteins operating from Escherichia coli to humans, *Adv. Enzymol. Relat. Areas Mol. Biol.*, 1992, **65**, 1–47.

27 E. L. Borths, *et al.*, In vitro functional characterization of BtuCD-F, the Escherichia coli ABC transporters for vitamin B_{12} uptake, *Biochemistry*, 2005, **44**, 16301–16309.

28 N. Cadieux, *et al.*, Identification of the Periplasmic Cobalamin-Binding Protein BtuF of Escherichia coli, *J. Bacteriol.*, 2002, **184**(3), 706–717.

29 O. Gat, *et al.*, The solute-binding component of a putative Mn(II) ABC transporter (MntA) is a novel Bacillus anthracis virulence determinant, *Mol. Microbiol.*, 2005, **58**(2), 533–551.

30 R. Janulczyk, S. Ricci and L. Bjorck, MtsABC is Important for Manganese and Iron Transport, Oxidative Stress Resistance and Virulence of Streptococcus pyogenes, *Infect. Immun.*, 2003, **71**(5), 2656–2664.

31 C. A. McDevitt, *et al.*, A Molecular Mechanism for Bacterial Susceptibility to Zinc, *PLoS Pathog.*, 2011, **7**(11), e1002357.

32 V. Rukhman, *et al.*, The MntC Crystal Structure Suggests that Import of Mn^{2+} in Cyanobacteria is Redox Controlled, *J. Mol. Biol.*, 2005, **348**(4), 961–969.

33 D. C. Desrosiers, *et al.*, The general transition metal (Tro) and Zn^{2+} (Znu) transporters in Treponema pallidum: analysis of metal specificities and expression profiles, *Mol. Microbiol.*, 2007, **65**(1), 137–152.

34 L. Tirado-Lee, *et al.*, Classification of a Haemophilus influenzae ABC Transporter HI1470/71 through its Cognate Molybdate Periplasmic Binding Protein, *J. Mol. Struct.*, 2011, **19**(11), 1701–1710.

35 E. Vigonsky, E. Ovcharenko and O. Lewinson, Two molybdate/tungstate ABC transporters that interact very

differently with their substrate binding proteins, *Proc. Natl. Acad. Sci. U. S. A.*, 2013, **110**(14), 5440–5445.

36 X. Sun, *et al.*, Crystal Structure and Metal Binding Properties of the Lipoprotein MtsA, Responsible for Iron Transport in Streptococcus pyogenes, *Biochemistry*, 2009, **48**(26), 6184–6190.

37 N. Eswar, *et al.*, in *Protein Structure Modeling with MODELLER, in Structural Proteomics*, ed. B. Kobe, M. Guss and T. Huber, Humana Press, 2008, pp. 145–159.

38 A. Roy, A. Kucukural and Y. Zhang, I-TASSER: a unified platform for automated protein structure and function prediction, *Nat. Protoc.*, 2010, **5**(4), 725–738.

39 T. Schwede, *et al.*, SWISS-MODEL: an automated protein homology-modeling server, *Nucleic Acids Res.*, 2003, **31**(13), 3381–3385.

40 R. A. Laskowski, *et al.*, {PROCHECK}: a program to check the stereochemical quality of protein structures, *J. Appl. Crystallogr.*, 1993, **26**, 283–291.

41 R. Luthy, J. U. Bowie and D. Eisenberg, Assessment of protein models with three-dimensional profiles, *Nature*, 1992, **356**(6364), 83–85.

42 M. Wiederstein and M. J. Sippl, ProSA-web: interactive web service for the recognition of errors in three-dimensional structures of proteins, *Nucleic Acids Res.*, 2007, **35**(web server issue), W407–W410.

43 M. Kalman and N. Ben-Tal, Quality assessment of protein model-structures using evolutionary conservation, *Bioinformatics*, 2010, **26**(10), 1299–1307.

44 M. C. Lawrence, *et al.*, The crystal structure of pneumococcal surface antigen PsaA reveals a metal-binding site and a novel structure for a putative ABC-type binding protein, *Structure*, 1998, **6**(12), 1553–1561.

45 R. M. Couñago, *et al.*, Imperfect coordination chemistry facilitates metal ion release in the Psa permease, *Nat. Chem. Biol.*, 2014, **10**(1), 35–41.

46 N. Li, *et al.*, Varied metal-binding properties of lipoprotein PsaA in Streptococcus pneumoniae, *JBIC, J. Biol. Inorg. Chem.*, 2014, **19**(6), 829–838.

47 C. J. Layton and H. W. Hellinga, Quantitation of protein–protein interactions by thermal stability shift analysis, *Protein Sci.*, 2011, **20**(8), 1439–1450.

48 M. D. Cummings, M. A. Farnum and M. I. Nelen, Universal Screening Methods and Applications of ThermoFluor®, *J. Biomol. Screening*, 2006, **11**(7), 854–863.

49 C. J. Layton and H. W. Hellinga, Thermodynamic Analysis of Ligand-induced Changes in Protein Thermal Unfolding Applied to High-throughput Determination of Ligand Affinities with Extrinsic Fluorescent Dyes, *Biochemistry*, 2010, **49**(51), 10831–10841.

50 A. Niedziela-Majka, *et al.*, High-throughput Screening of Formulations to Optimize the Thermal Stability of a Therapeutic Monoclonal Antibody, *J. Biomol. Screening*, 2015, **20**(4), 552–559.

51 O. Lewinson, *et al.*, A distinct mechanism for the ABC transporter BtuCD-BtuF revealed by the dynamics of complex formation, *Nat. Struct. Mol. Biol.*, 2010, **17**(3), 332–338.

52 J.-S. Woo, *et al.*, X-ray structure of the Yersinia pestis heme transporter HmuUV, *Nat. Struct. Mol. Biol.*, 2012, **19**(12), 1310–1315.

53 B. K. Kay, M. P. Williamson and M. Sudol, The importance of being proline: the interaction of proline-rich motifs in signaling proteins with their cognate domains, *FASEB J.*, 2000, **14**(2), 231–241.

54 Y. Nevo and N. Nelson, The NRAMP family of metal-ion transporters, *Biochim. Biophys. Acta, Mol. Cell Res.*, 2006, **1763**(7), 609–620.

55 F. Abate, *et al.*, Apo, Zn(2+)-bound and Mn(2+)-bound structures reveal ligand-binding properties of SitA from the pathogen Staphylococcus pseudintermedius, *Biosci. Rep.*, 2014, **34**(6), e00154.

56 A. J. Rice, A. Park and H. W. Pinkett, Diversity in ABC transporters: Type I, II and III importers, *Crit. Rev. Biochem. Mol. Biol.*, 2014, **49**(5), 426–437.

57 M. C. Clifton, *et al.*, In vitro Reassembly of the Ribose ATP-binding Cassette Transporter Reveals a Distinct Set of Transport Complexes, *J. Biol. Chem.*, 2015, **290**(9), 5555–5565.

58 P. A. B. Ronnie, *et al.*, A structural classification of substrate-binding proteins, *FEBS Lett.*, 2010, **584**(12), 2606–2617.

59 K. Hollenstein, D. C. Frei and K. P. Locher, Structure of an ABC transporter in complex with its binding protein, *Nature*, 2007, **446**(7132), 213–216.

60 R. N. Hvorup, *et al.*, Asymmetry in the structure of the ABC transporter binding protein complex BtuCD-BtuF, *Science*, 2007, **317**, 1387–1390.

61 M. L. Oldham and J. Chen, Crystal Structure of the Maltose Transporter in a Pretranslocation Intermediate State, *Science*, 2011, **332**(6034), 1202–1205.

62 A. Krogh, *et al.*, Predicting transmembrane protein topology with a hidden Markov model: application to complete genomes1, *J. Mol. Biol.*, 2001, **305**(3), 567–580.

63 K. P. Locher, A. T. Lee and D. C. Rees, The E. coli BtuCD structure: a framework for ABC transporter architecture and mechanism, *Science*, 2002, **296**(5570), 1091–1098.

64 N. S. Kadaba, *et al.*, The high-affinity E. coli methionine ABC transporter: structure and allosteric regulation, *Science*, 2008, **321**, 250–253.

65 G. F. Ames, *et al.*, Liganded and unliganded receptors interact with equal affinity with the membrane complex of periplasmic permeases, a subfamily of traffic ATPases, *J. Biol. Chem.*, 1996, **271**(24), 14264–14270.

66 C. E. Liu, P.-Q. Liu and G. F.-L. Ames, Characterization of the Adenosine Triphosphatase Activity of the Periplasmic Histidine Permease, a Traffic ATPase (ABC Transporter), *J. Biol. Chem.*, 1997, **272**(35), 21883–21891.

67 K. Nikaido and G. F.-L. Ames, One Intact ATP-binding Subunit is Sufficient to Support ATP Hydrolysis and Translocation in an ABC Transporter, the Histidine Permease, *J. Biol. Chem.*, 1999, **274**(38), 26727–26735.

68 J. Chen, *et al.*, Trapping the transition state of an ATP-binding cassette transporter: evidence for a concerted mechanism of maltose transport, *Proc. Natl. Acad. Sci. U. S. A.*, 2001, **98**(4), 1525–1530.

69 A. L. Davidson, H. A. Shuman and H. Nikaido, Mechanism of maltose transport in Escherichia coli: transmembrane signaling by periplasmic binding proteins, *Proc. Natl. Acad. Sci. U. S. A.*, 1992, **89**(6), 2360–2364.

70 N. Tal, E. Ovcharenko and O. Lewinson, A single intact ATPase site of the ABC transporter BtuCD drives 5% transport activity yet supports full in vivo vitamin B12 utilization, *Proc. Natl. Acad. Sci. U. S. A.*, 2013, **110**(14), 5434–5439.

71 S. R. Eddy, Profile hidden Markov models, *Bioinformatics*, 1998, **14**(9), 755–763.

72 S. F. Altschul, *et al.*, Gapped BLAST and PSI-BLAST: a new generation of protein database search programs, *Nucleic Acids Res.*, 1997, **25**(17), 3389–3402.

73 R. C. Edgar, MUSCLE: a multiple sequence alignment method with reduced time and space complexity, *BMC Bioinf.*, 2004, **5**, 113.